

Visual Neural Decoding via Improved Visual-EEG Semantic Consistency

Hongzhou Chen¹, Lianghua He^{2,1}, Yihang Liu¹, Longzhen Yang¹

¹The Department of Electronic and Information Engineering, Tongji University, Shanghai 201804, China.

²Shanghai Eye Disease Prevention and Treatment Center, Shanghai 200040, China.

{chenhongzhou, Helianghua, 2111131, yanglongzhen}@tongji.edu.cn

Abstract—Visual neural decoding refers to the process of extracting and interpreting original visual experiences from human brain activity. Recent advances in metric learning-based EEG visual decoding methods have delivered promising results and demonstrated the feasibility of decoding novel visual categories from brain activity. However, methods that directly map EEG features to the CLIP embedding space may introduce mapping bias and cause semantic inconsistency among features, thereby degrading alignment and impairing decoding performance. To further explore the semantic consistency between visual and neural signals. In this work, we construct a joint semantic space and propose a Visual-EEG Semantic Decouple Framework that explicitly extracts the semantic-related features of these two modalities to facilitate optimal alignment. Specifically, a cross-modal information decoupling module is introduced to guide the extraction of semantic-related information from modalities. Then, by quantifying the mutual information between visual image and EEG features, we observe a strong positive correlation between the decoding performance and the magnitude of mutual information. Furthermore, inspired by the mechanisms of visual object understanding from neuroscience, we propose an intra-class geometric consistency approach during the alignment process. This strategy maps visual samples within the same class to consistent neural patterns, which further enhances the robustness and the performance of EEG visual decoding. Experiments on a large Image-EEG dataset show that our method achieves state-of-the-art results in zero-shot neural decoding tasks.

Index Terms—EEG-based visual neural decoding, multimodal contrastive learning (MCL), semantic consistency, mutual information maximization.

I. INTRODUCTION

ACCURATE decoding of human visual information from brain activity holds significant potential to propel advancements in cognitive neuroscience [1], [2], [3] and the field of computer vision [4], [5], [6]. The key to achieving effective decoding lies in how to extract semantic information related to stimulus images from complex neural activity. Traditionally, the decoding process of electroencephalogram (EEG) or functional magnetic resonance imaging (fMRI) involves learning a mapping function [7], [8], [9], [10] to associate extracted neural activity features with predefined class labels to achieve recognition of specific patterns. However, due to the lack of effective biological plausibility and the difficulty in extracting semantic components from limited neural activity, these predefined label methods still face significant challenges in accurately decoding visual neural signals and generalizing them to novel categories [11], [12].

In recent research on decoding human visual neural representations, researchers have begun incorporating multimodal data [13], such as images or text [14], [15], [16], aimed at mitigating the scarcity of brain activity data and aligning neural signals with other modalities for decoding or reconstruction [17], [18], [19]. Recent EEG-based neural decoding methods deliver promising results in decoding natural images for object recognition. This is accomplished by mapping extracted EEG features into the pre-trained model embedding space for aligning the priors, followed by decoding EEG signals using a metric learning-based approach. NICE [16] employs a self-supervised framework to align EEG features and CLIP image embeddings through multimodal contrastive learning (MCL), and this end-to-end training approach achieves outstanding decoding performance. Subsequently, Li *et al.* [18] proposed an effective EEG encoder called ATM, which can extract meaningful spatio-temporal representations of EEG signals, further matching them with image embeddings. However, these methods demonstrate that after MCL, as illustrated in Fig. 1(a) and Fig. 1(b), the embeddings of EEG samples, processed through the encoder, are located in completely separate regions from those of the CLIP image and text embeddings on a hypersphere. This phenomenon is known as the *modality gap* [20], which creates challenges in accurately matching EEG embeddings with image categories and results in a decline in the model’s performance for the classification or retrieval task.

Additionally, MCL-based approaches optimize modality alignment by maximizing cosine similarity for positive pairs and minimizing it for negative pairs. The visual features or text features used for alignment are extracted from pre-trained models, where not all dimensions are semantically related to the high-level features of object recognition in EEG. Especially when the priors are fixed, directly calculating the similarity between modality features might lead to a lack of effective contextual understanding. Consequently, the network might fit features that do not evoke neural responses related to the high-level semantics of object recognition, such as irrelevant image color, brightness, background, or overfitting to white noise, particularly in the case of high signal-to-noise ratio signals like EEG.

To focus on the semantic consistency between stimulus images and neural signals. Du *et al.* [14] proposed a trimodal Brain-Visual-Linguistic representation learning approach, named BraVL, which focuses on modeling the re-

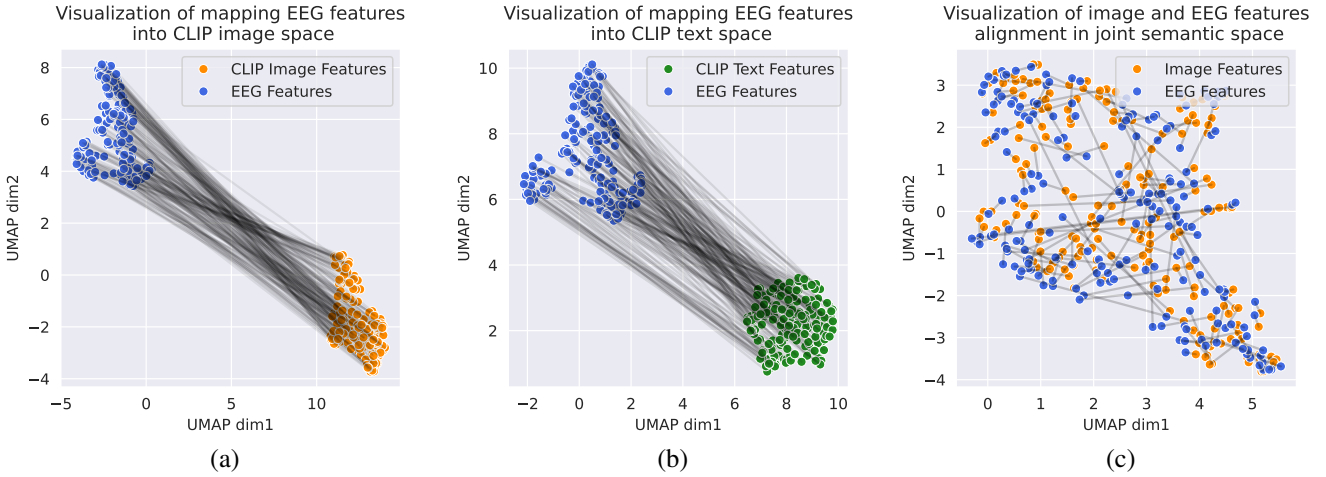


Fig. 1. Illustration of UMAP [23] 2D visualization of training CLIP images, text, and EEG features aligned on a hypersphere with multimodal contrastive training. (a) and (b) demonstrate the direct mapping of EEG samples into the fixed pre-trained CLIP space along with the corresponding alignment of image and text features, highlighting the apparent modality gap between features. (c) Reproject CLIP image features and EEG embedding into joint semantic space, and visualize the aligned features afterward.

relationships between brain activity and multimodal semantic knowledge. BraVL employs a generative model, and the MoPoE [21] formulation to infer a consistent trimodal representation and incorporates intra- and inter-modality mutual information (MI) regularization to refine the consistency of the joint representation. Drawing on insights from the brain representing concepts using a similar Locality-Sensitive Hashing (LSH) strategy [22], Chen *et al.* [11] proposed a fuzzy matching paradigm, which formulates one (neural signals) to many (diverse images within the same class) loss function, which compels the model to prioritize capturing high-level semantic information. However, since there is a significant discrepancy between neural signals and multimodal features, coupled with the inherent noise and artifacts present in neural signals, these semantic-awareness or MCL-based methods do not ensure a close semantic relationship among all aligned feature pairs. Due to the abundance of semantic-unrelated information between neural and multimodal features, direct feature mapping or alignment may lead to bias in learning semantic consistency features between stimulus images and neural signals, potentially resulting in negative transfer to novel categories and impairing decoding performance.

To tackle the above two issues and further explore the semantic consistency between visual images and neural signals. Firstly, we reproject these two embeddings into a joint semantic space, thereby reducing the disparities in their distribution across the original feature spaces of modalities. As illustrated in Fig. 1(c), the joint semantic space reduces the distributional gaps between modality samples, making it easier to match cross-modal samples. Secondly, we propose a Visual-EEG Semantic Decouple Framework, called VE-SDN, which separates the modality features into semantic-related and domain-specific information. We enhance the semantic consistency by explicitly decoupling the semantic-related components of visual images and EEG, and directly aligning these components. To guide the extraction of semantic-related information from modalities, we propose a mutual information

maximization-minimization adversarial learning-based method to decouple the original features. Then, to advance the semantic consistency between visual and EEG, we utilize cross-modal cyclic reconstruction to further improve the semantic correlations between these two and avoid the degenerate case of domain features during the training process. Our quantitative results indicate that higher mutual information between visual images and EEG features during training correlates with improved generalization ability and decoding performance, both at intra-subject and inter-subject levels. Furthermore, similarly inspired by the locality-sensitive homology [22] and invariance of core object recognition in the brain [24], we propose a geometric consistency loss to maintain the intra-class consistency during the MCL, which ensures that distinct visual samples of the same class maintain consistency with their corresponding neural representations. Concretely, this constraint retains a consistent Euclidean distance of modality gap between visual samples and the corresponding EEG prototype. By incorporating this geometric consistency constraint, we simulate the encoding of visual concepts in the human cognitive space, thereby enhancing the robustness of alignment. In summary, our contributions are as follows:

- 1) In order to explicitly explore the semantic correlation between visual and brain activity. We propose a Visual-EEG Semantic Decouple Framework (VE-SDN), which decouples the semantic-related parts of visual image and EEG to achieve effective semantic alignment.
- 2) By quantifying the estimated MI values between image and EEG features, we found that both intra-subject and inter-subject with higher classification accuracy often exhibit higher MI values. This insight may provide guidance for designing more effective neural decoding methods.
- 3) Combined with achieving inter-modality semantic consistency, we propose an intra-class geometric consistency approach, further enhancing the robustness and decoding accuracy of EEG signals.
- 4) Our results indicate that improving the semantic consis-

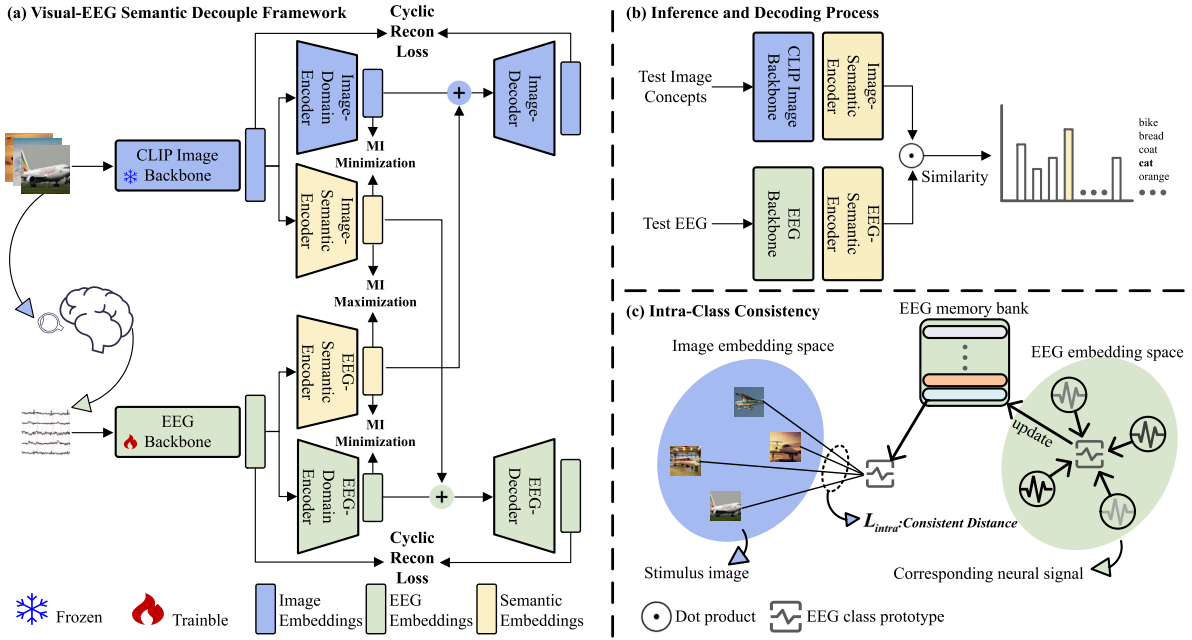


Fig. 2. The overview of the proposed Visual-EEG Semantic Decouple Framework (VE-SDN). (a) The main pipeline for semantic decoupling of stimulus images and EEG signals. (b) The inference and decoding process of our proposed VE-SDN. (c) Intra-class geometric consistency constraint in the process of the alignment of semantic-related features.

tency between the stimulus images and neural signals can enhance the performance of EEG-based visual category decoding. Experiments conducted on a large-scale Visual-EEG dataset [25] demonstrate that our method achieves state-of-the-art results in subject-dependent zero-shot neural decoding task.

II. RELATED WORK

A. EEG-Based Visual Neural Decoding

Owing to the high temporal resolution and portability of EEG [26], [9], the decoding of EEG signals evoked by visual stimuli is increasingly emphasized in research [6], [12], [16], [13], [27], [28]. Early visual stimuli-evoked EEG signal decoding involved a limited and small number of object categories, with a low recognition accuracy [29]. Subsequently, Spampinato *et al.* [6] record EEG signals for 40 classes of visual object stimuli and propose an LSTM-based method that achieved an accuracy of 82.9% in classification tasks. Then, this classification result was further improved by [13], and it introduced a multimodal learning approach to perform saliency detection on visual images and EEG signals. However, the above block-based experimental paradigm design leads to flaws in the data itself [28], resulting in the classification of temporal artifacts of the data rather than the stimulus-related activity. Recent research has collected a large-scale Visual-EEG dataset [25], [30] with 16,740 image stimuli of 1,854 concepts using the RSVP paradigm [31], [32] and showing the feasibility of encoding images to EEG signals and the distinguishability between categories. Du *et al.* [14], building on this work, proposed a model based on Brain-Visual-Linguistic trimodal representation, demonstrating that

decoding novel visual categories from human brain activity is practically feasible. Song *et al.* [16] propose a multimodal contrastive learning approach that improves the accuracy of zero-shot neural decoding for EEG. Later, due to the weaknesses of the EEG encoder, Li *et al.* [18] proposed a powerful EEG encoder called ATM, which effectively aligns with image embeddings and further improves the accuracy of EEG visual decoding. In our work, We explore the semantic consistency between visual information and neural signals, further aligning visual images and EEG in a joint semantic space through the explicit extraction of semantic-related parts to achieve better decoding performance.

B. Multimodal Contrastive Learning

Multimodal Contrastive Learning aims to maximize the similarity between matched multimodal pairs and against all the mismatched pairs. This alignment method enables the learned representations to excel in multiple downstream tasks and demonstrate strong zero-shot classification capabilities. Recent research indicates that there is a phenomenon known as the *modality gap* during the process of multimodal contrastive learning, which refers to the representations from different modalities that are found to reside in distinct regions in the joint representation space [33], [34], [35]. [20] demonstrates that reducing the modality gap may enhance the model performance in zero-shot classification tasks. While [36] shows that reducing the modality gap generally does not yield optimal results for downstream predictive tasks and advocates the construction of a meaningful latent modality structure. CyCLIP [37] constructs a geometric constraint in multimodal representation spaces with cyclic consistency to improve performance on downstream predictive tasks. In our

work, we construct a joint semantic space and align the semantic consistency features to reduce the disparities between modality distributions. Instead of further reducing the modality gap, we apply a neuroscience-inspired intra-class geometric consistency of modality gap to prevent instability in alignment and overfitting to a particular type of sample on the hypersphere. This approach constructs an improved latent modality structure, enhancing the robustness of the model.

III. METHOD

A. Problem Definition: Zero-Shot Neural Decoding

The task setup follows [16], employing only visual stimuli image and EEG pairs without introducing additional data. Formally, given a seen class dataset $D^{seen} = \{(x_b, x_v, y | x_b \in X_b, x_v \in X_v, y \in Y)\}$, where X_b represents the set of EEG signals, X_v represents the set of stimuli images, Y denotes the corresponding seen class labels. The seen class labels span from 1 to S , $y \in L = \{1, \dots, S\}$. Given an unseen class dataset $D^{unseen} = \{(x_b^u, x_v^u, y^u | x_b^u \in X_b^u, x_v^u \in X_v^u, y^u \in Y^u)\}$, where X_b^u, X_v^u, Y^u represents the set of unseen class EEG, images, and class labels, respectively. The unseen class labels span from $S + 1$ to $S + U$, $y^u \in L^u = \{S + 1, \dots, S + U\}$. The seen and unseen classes are mutually exclusive, i.e., $L \cap L^u = \emptyset$. The unseen class features X_b^u, X_v^u are not available during training. At the testing phase, X_v^u serves as novel concepts for new visual categories, with the decoding of EEG features X_b^u achieved by calculating their similarity to these visual concepts.

B. Cross-Modal Semantic Information Decoupling

1) *Semantic and Domain Feature Extraction*: The total pipeline of our model VE-SDN is illustrated in Fig. 2 (a). We first utilize a fixed pre-trained CLIP [35] Vision Transformer (ViT) and a trainable ATM-S [18] EEG encoder to extract embeddings from the raw stimulus images and preprocessed EEG signals, denoted as $h_v \in \mathbb{R}^{N \times 1024}$ and $h_b = F_b(x_b) \in \mathbb{R}^{N \times F}$ from the neural data $x_b \in \mathbb{R}^{N \times C \times T}$, where F_b, F, C, T represents the EEG backbone, and the feature dimension, the channel and the time point of EEG signals, respectively. Then, input the extracted image and EEG embeddings into their respective modality's semantic and domain encoder, denoted as:

$$z_v^s = \Phi_v(h_v) \quad z_v^d = \Psi_v(h_v) \quad (1)$$

$$z_b^s = \Phi_b(h_b) \quad z_b^d = \Psi_b(h_b) \quad (2)$$

where $z_v^s, z_v^d, z_b^s, z_b^d$ represent the semantic and domain parts of images, EEG embeddings respectively. Φ, Ψ are the semantic and domain encoders.

2) *Mutual Information Minimization*: We devise an information decoupling module, assuming that each modality's semantic and domain parts are uncorrelated. Information decoupling is achieved by minimizing the upper bound of mutual information of each modality, estimated using the CLUB [38], formulated as:

$$I(z_m^d; z_m^s) \leq E_{p(z_m^d, z_m^s)}[\log p(z_m^s | z_m^d)] - E_{p(z_m^d) p(z_m^s)}[\log p(z_m^s | z_m^d)] \quad (3)$$

where $I(z_m^d; z_m^s), m \in \{v, b\}$ are the mutual information between the two modalities semantic and domain features. Since the conditional distribution $p(z^s | z^d)$ is intractable in practice, we employ a variational inference approach, parameterizing a conditional distribution $q(z^s | z^d)$ with a neural network θ to approximate the upper bound of mutual information with samples $\{(z_{m,i}^s, z_{m,i}^d)\}_{i=1}^N$, which is formulated as:

$$\hat{I}(z_m^d; z_m^s) = \frac{1}{N} \sum_{i=1}^N [\log q_{\theta_m}(z_{m,i}^s | z_{m,i}^d) - \frac{1}{N} \sum_{j=1}^N \log q_{\theta_m}(z_{m,j}^s | z_{m,i}^d)] \quad (4)$$

Besides, according to [38] Theorem 3.2, we need to minimize the discrepancy between the distribution $p(z^s | z^d)$ and the variational distribution $q_{\theta}(z^s | z^d)$, to ensure that $\hat{I}(z^d; z^s)$ still represents a reliable upper bound of mutual information. Specifically, we adopt the KL divergence to measure the difference between two distributions, denoted as:

$$\min_{\theta} KL(p(z^s, z^d) || q_{\theta}(z^s, z^d)) = \min_{\theta} E_{p(z^d, z^s)}[\log p(z^d | z^s)] - E_{p(z^d, z^s)}[\log q_{\theta}(z^d | z^s)] \quad (5)$$

In Eq. (5), the first term has no relation with parameter θ , thus to minimize the $KL(p(z^s, z^d) || q_{\theta}(z^s, z^d))$ can be achieved by minimizing the negative log-likelihood with samples $\{(z_{m,i}^s, z_{m,i}^d)\}_{i=1}^N$, denoted as:

$$L(\theta) = -\frac{1}{N} \sum_{i=1}^N \log q_{\theta}(z_{m,i}^d | z_{m,i}^s) \quad (6)$$

which is the unbiased estimation of $E_{p(z^d, z^s)}[\log q_{\theta}(z^d | z^s)]$. During training, we decouple the semantic and domain parts by minimizing the estimated mutual information between the semantic and domain features within the modalities of image and EEG embeddings, denoted as:

$$L_{MI} = \hat{I}(z_v^d; z_v^s) + \hat{I}(z_b^d; z_b^s) \quad (7)$$

The approximate neural networks θ for the two modalities and the main network are trained alternately during the optimization process.

3) *Mutual Information Maximization*: To determine the cross-modal semantic consistency features between the extracted image and EEG embeddings. We aim to maximize the mutual information between semantic-related parts z_v^s and z_b^s . Following the approach proposed in [39], our goal is to maximize the lower bound on mutual information by minimizing the InfoNCE loss, as follows:

$$L_{con} = -\frac{1}{2N} \sum_{i=1}^N \left[\log \frac{\exp(f(z_{v,i}^s, z_{b,i}^s)/\tau)}{\sum_{j=1}^N \exp(f(z_{v,i}^s, z_{b,j}^s)/\tau)} + \log \frac{\exp(f(z_{b,i}^s, z_{v,i}^s)/\tau)}{\sum_{j=1}^N \exp(f(z_{b,i}^s, z_{v,j}^s)/\tau)} \right] \quad (8)$$

where $f(\cdot, \cdot)$ represents the cosine similarity, and τ represents the temperature parameter. We explicitly decouple the semantic-related features of visual and neural activity through a form of adversarial learning, employing mutual information

maximization-minimization and aligning the modalities via MCL.

4) *Inter-modality Semantic Consistency*: To avoid the degenerate case of modality domain features, which involves learning non-informative noises, and to further enhance the semantic consistency of visual and EEG semantic features. We employ cyclic consistency signal reconstruction, by reconstructing the original visual image features using visual domain parts combined with the EEG semantic parts and vice versa, denoted as:

$$L_{recon} = \frac{1}{2}(MSE(h_v, D_v(z_v^d, z_b^s)) + MSE(h_b, D_b(z_b^d, z_v^s))) \quad (9)$$

where $MSE(\cdot, \cdot)$ represents Mean-Squared loss, and $D_v(\cdot, \cdot), D_b(\cdot, \cdot)$ represents the decoder of visual and EEG part, and in this work, the method for concatenating multimodal features employs direct feature addition. By enforcing semantic alignment through cyclic consistency reconstruction, the representation of two modalities is compelled to contain consistent information, thereby enhancing the extraction of semantic-related features.

C. Intra-Class Geometric Consistency

As [24] proposes, although the same object triggers completely different patterns of retinal responses, the visual system's task is to somehow equate all these different response patterns. Therefore, in the joint semantic space, we aim to establish the equivalence among all visual samples of the same category along with their corresponding neural responses. Specifically, we define each visual concept in neural response as a category of EEG prototype. Before the training begins, we randomly initialize all categories of EEG prototypes $C_b = \{c_1, c_2, \dots, c_k\}$, and in each training mini-batch, we calculate the average EEG semantic features \bar{z}_b^s , as follows:

$$\bar{z}_{b_k}^s = \frac{1}{\|Y_{b_k}\|} \sum_{z_b^s \in Y_{b_k}} z_b^s \quad (10)$$

where $\bar{z}_{b_k}^s$ represents the clustering center of the EEG semantic features for class k , while Y_{b_k} is the set of EEG semantic features with label k and $\|Y_{b_k}\|$ represents the corresponding number of samples.

1) *Prototype momentum update*: We utilize a memory bank to store the prototypes of EEG semantic features, and dynamically update the EEG prototypes using the EMA method. After calculating the EEG semantic features in each mini-batch, we update C_b based on the average feature vector \bar{z}_b^s of the samples from that class, denoted as:

$$c_k \leftarrow \alpha c_k + (1 - \alpha) \bar{z}_{b_k}^s \quad (11)$$

where α is momentum update coefficient, and the $\bar{z}_{b_k}^s$ is the average feature of class k in a mini-batch.

2) *Intra-class Geometric Consistency Loss*: The visual system is capable of unifying different response patterns of the same object in a certain way, thereby enabling the brain to precisely identify and retrieve these visual samples. Similarly, to enhance the decoding accuracy of neural signals

Algorithm 1: Training Algorithm of the VE-SDN

Input: Training Image-EEG pairs D^{seen} ; Extracted image features h_v ; Learnable temperature parameter τ ; Hyper-parameters: $\lambda_1, \lambda_2, \lambda_3, \alpha$.

Output: The EEG backbone F_b ; The EEG-semantic encoder Φ_b ; The image-semantic encoder Φ_v .

```

1 Initialize EEG prototypes memory bank  $C_b$  and
  network parameters EEG parts  $\{F_b, \Phi_b, \Psi_b, \theta_b, D_b\}$ ;
  Visual parts  $\{\Phi_v, \Psi_v, \theta_v, D_v\}$ .
2 for each training iteration do
3   for sampled a mini-batch  $\{h_{v,i}, x_{b,i}, y\}_{i=1}^N$  do
4     Compute batch EEG features  $h_b = F_b(x_b)$ ;
5     Compute  $z_v^s, z_v^d, z_b^s, z_b^d$  by Eq. (1) and Eq. (2);
6     Normalize features:  $z_v^s, z_v^d, z_b^s, z_b^d \leftarrow$ 
      Norm( $z_v^s$ ), Norm( $z_v^d$ ), Norm( $z_b^s$ ), Norm( $z_b^d$ );
7     Compute  $\bar{z}_b^s$  by Eq. (10);
8     Momentum update  $C_b$  by Eq. (11);
9     for  $k \leftarrow 1$  to  $n_{logli}$  do
10      Calculate Log-likelihood  $L(\theta_v), L(\theta_b)$  using
        each modality's  $z^s$  and  $z^d$  by Eq. (6);
11      Update approximate network  $\theta_v, \theta_b$  by
        maximizing  $L(\theta_v), L(\theta_b)$ ;
12      Compute  $L_{intra}$  by Eq. (12) and Eq. (13);
13      MI Minimization following Eq. (7);
14      MI Maximization following Eq. (8);
15      Cyclic reconstruction following Eq. (9);
16      Compute  $L = L_{con} + \lambda_1 L_{MI} + \lambda_2 L_{recon}$ 
17       $+ \lambda_3 L_{intra}$ ;
18      Update the main network of EEG and visual
        parts;
```

in our system, we further enhance consistency in the distance gaps between visual samples of the same category and their corresponding EEG prototypes on the hypersphere. Concretely, for a mini-batch visual semantic samples z_v^s , we calculate the modality gap between each sample and its corresponding EEG prototype c_k and compute the average intra-class distance within each category k :

$$\bar{d}_k = \frac{1}{\|Y_{v_k}\|} \sum_{z_v^s \in Y_{v_k}} d(z_v^s, c_k) \quad (12)$$

where $d(\cdot)$ represents the Euclidean distance, while \bar{d}_k represents the average distance from intra-class visual samples to the neural prototype, and Y_{v_k} is the set of visual semantic features with label k . To enhance the intra-class consistency, we devise a geometric consistency loss that aims to attain the uniform distance from various visual samples to the neural prototype. This is achieved by minimizing the variance of the distances d_k within the same category, effectively equating all these response patterns, which is denoted as:

$$L_{intra} = \sum_{j=1}^k \frac{1}{\|Y_{v_j}\|} \sum_{z_v^s \in Y_{v_j}} \|d(z_v^s, c_j) - \bar{d}_j\|_2 \quad (13)$$

TABLE I

ABLATION STUDIES IN THE 200-WAY ZERO-SHOT CLASSIFICATION TASK. REPORT THE TOP-1 AND TOP-5 ACCURACY (%) OF EACH COMPONENT OF OUR PROPOSED METHODS. WE CONDUCTED TRAINING AND TESTING SEPARATELY ON TEN SUBJECTS AND CALCULATED THE AVERAGE ACCURACY.

Method	Subject 1		Subject 2		Subject 3		Subject 4		Subject 5		Subject 6		Subject 7		Subject 8		Subject 9		Subject 10		Average	
	top-1	top-5	top-1	top-5	top-1	top-5	top-1	top-5	top-1	top-5	top-1	top-5	top-1	top-5	top-1	top-5	top-1	top-5	top-1	top-5	top-1	top-5
CLIP-Con	24.70	56.05	26.05	58.00	29.15	61.85	32.95	63.50	20.85	49.75	27.50	63.75	27.65	60.50	38.60	69.75	28.50	62.55	32.00	66.85	28.80	61.26
Joint-Con	28.00	63.20	29.90	64.80	35.00	67.25	32.75	73.15	28.65	58.00	33.30	61.65	33.35	65.15	50.35	77.25	36.35	67.65	39.10	71.90	34.68	67.00
Joint-Con+Intra	28.05	61.50	35.65	66.35	39.05	72.55	41.20	70.60	23.95	56.15	35.50	71.15	31.35	65.55	49.95	78.80	35.35	70.40	42.25	74.55	36.23	68.76
VE-SDN	32.55	63.65	34.40	69.90	38.65	73.45	39.75	72.00	29.35	58.60	34.45	68.80	34.50	68.30	49.30	79.75	39.00	69.60	39.80	75.30	37.18	69.94
VE-SDN+Intra	35.05	65.95	34.20	66.75	38.40	73.60	40.30	70.75	28.10	57.75	34.60	67.20	35.50	66.80	47.85	79.30	43.90	71.30	44.95	77.00	38.29	69.64

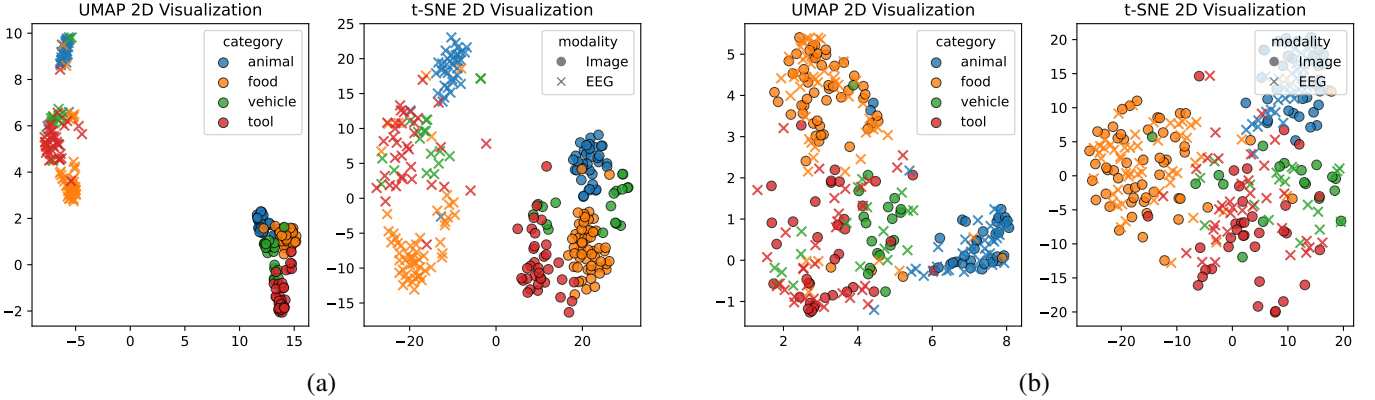


Fig. 3. 2D UMAP and t-SNE [40] visualization of four categories: animal, food, vehicle, and tool of subject 8 test visual image and EEG features. (a) Visualization of CLIP-Con two modality embeddings. (b) Visualization of Joint-Con two modality embeddings.

On the one hand, by explicitly reducing the variability of intra-class sample distances, we implicitly bolster cohesion within classes and simultaneously improve the semantic consistency between visual and neural responses. On the other hand, by implementing methods akin to regularization, we mitigate overfitting to specific intra-class samples, thereby reducing the intra-class variability and enhancing the robustness of the model.

D. Training and Inference

Algorithm 1 shows the pseudocode of model training. In the training process, there are two approximate networks θ_b, θ_v alternating optimization with the main network, and the loss denoted as:

$$L_{\loglikei} = L(\theta_b) + L(\theta_v) \quad (14)$$

The overall loss for our main network is defined as :

$$L = L_{con} + \lambda_1 L_{MI} + \lambda_2 L_{recon} + \lambda_3 L_{intra} \quad (15)$$

where λ_1, λ_2 and λ_3 are hyperparameters.

In the decoding process, we use the visual image as concept templates. Then, input the test EEG signals and visual templates into the model to get the semantic-related features. We get the results by calculating the cosine similarity between test EEG features and visual templates, which is denoted as:

$$P_{zsl}(x_b^u) = \max_j < z_b^s \cdot z_{v_j}^s >_{j=S+1}^{S+U} \quad (16)$$

IV. EXPERIMENTS

A. Datasets and Implementation Details

1) *Datasets and Preprocessing*: ThingsEEG [25] is a large EEG dataset that employs the RSVP paradigm and includes 10 human subjects. The EEG data are collected using 64-channel EASYCAP equipment. The training set includes 1654 image classes with each class 10 images, and each image presents 4 times (1654 concepts \times 10 images \times 4 repetitions) per subject. The test set includes 200 image classes with each class only 1 image, and each image presents 80 times (200 concepts \times 1 image \times 80 repetitions) per subject. In this work, for EEG preprocessing, we adopt the same method as [16]. The EEG data are segmented into 0-1000 ms trials post-stimulus onset, with baseline correction using the prior 200 ms average. The data retain all electrodes, are downsampled to 250 Hz, and undergo multivariate noise normalization using the training data. Also, we averaged each EEG repetition to ensure a high signal-to-noise ratio for a total of 16540 training samples and 200 test samples per subject. For stimulus images, we utilize fixed pre-train CLIP-ViT-H-14¹ as the image backbone to extract the visual features.

2) *Implementation Details*: Our experiments were conducted on a single A6000 GPU using Pytorch. The EEG backbone we apply is ATM-S [18], which is currently the SOTA EEG backbone in the 200-way zero-shot neural decoding task. We

¹<https://huggingface.co/laion/CLIP-ViT-H-14-laion2B-s32B-b79K>

employ a two-layer MLP with a GELU activation function as the visual and EEG semantic and domain encoder, where both the semantic-related and domain-related feature sets are configured with 512 dimensions. The model is trained for 50 epochs by using the AdamW [41] optimizer with a learning rate of $3e-4$ and batch size of 1024, while the initial temperature parameter set is 0.07. The hyper-parameters $\lambda_1, \lambda_2, \lambda_3, \alpha$ we set is 1, 2, 0.5, 0.5, for all subjects, respectively.

B. Ablation Study

In this section, we systematically investigate the impact of each component of our proposed methods to understand their contributions to the overall performance. Experiments were conducted individually on ten subjects to test the decoding performance. We evaluated the component using the 200-way zero-shot classification task, measuring both top-1 and top-5 accuracy. The results are detailed in Table I.

1) *Contrastive Learning in CLIP Image Space*: We utilize the EEG part semantic encoder (a two-layer MLP with GELU activation) as the projector to directly map the extracted embeddings to the CLIP image space while using a contrastive loss (ConLoss) in Eq. (8) for alignment. During this training, the image embeddings from CLIP remain unchanged. The average top-1 accuracy of ten subjects, as shown in Table I CLIP-Con. The visualization of two modality test samples embedding, using subject 8, which has the best performance in feature representation learning, is shown in Fig. 3(a); we selected test pairs from four categories out of 200 test classes and found that in the embedding space of CLIP-Con, intra-semantic class clusters were formed for each modality. However, due to the presence of the modality gap, the untrained sample distribution of the two modalities did not overlap in regions, making sample matching difficult.

2) *Contrastive Learning in Joint Semantic Space*: We argue that directly mapping EEG embeddings into the pre-train CLIP image space leads to suboptimal semantic alignment and generalization ability. Therefore, we employ the visual part semantic encoder (a two-layer MLP with GELU activation) to reproject the corresponding CLIP image embeddings into a 512-dimensional joint semantic space. Similarly, we process the EEG embeddings in the same manner and then use ConLoss for alignment. The results from Joint-Con demonstrate that reprojecting CLIP image embeddings into a joint Visual-EEG space improves the top-1 and top-5 accuracy by large margins of 5.88% and 5.74%, respectively. This reprojection approach eliminates a certain bias associated with direct mapping and, as shown in Fig. 3(b), eradicates the modality gap in the visual-EEG joint space. Consequently, it achieves modality-agnostic intra-semantic class clustering, bringing visual and EEG samples of the same class closer together in the test sets.

3) *Visual-EEG Semantic Decouple Framework*: In response to the significant modality discrepancy for image and EEG features, we propose an explicit semantic decoupling framework. By employing the MI-based information decoupling method and inter-modality semantic consistency, we align the features with high semantic correlation and the detailed analysis in

Sec. IV-C. The results of VE-SDN show that, compared to direct training in joint semantic space, our proposed VE-SDN improves classification accuracy for almost every subject. Overall, it boosts the average top-1 and top-5 accuracy by 2.50% and 2.94%, respectively.

4) *Intra-class Geometric Consistency*: The training process of EEG signals is highly unstable and prone to overfitting. To further enhance the robustness, we propose a neuroscience-inspired intra-class geometric consistency that equates the modality gap of all image samples to the EEG class prototype. This prevents instability caused by rapid changes in the distance of modal distributions in the semantic space, and as analysis is in Sec. IV-E. The results in Table I indicate that adding intra-class constraints to the training process can enhance overall classification accuracy in both methods Joint-Con and VE-SDN.

C. Analysis on Semantic Information Decoupling

In this section, we evaluate the Cross-Modal Semantic Information Decoupling Module, which explicitly extracts the semantic-related features for visual images and EEG. To quantify the mutual information between the semantic-related parts of images and EEG, we additionally trained an approximate network to estimate their mutual information, while this network does not participate in the gradient updates of the main network.

Firstly, as shown in Fig. 4(a), the MI values between the semantic and domain-related parts of the image and EEG decrease from initial fluctuations as training progresses, indicating a gradually weakening correlation between them. As shown in Fig. 5(a), the MI values between the semantic-related features of the two modalities gradually increase during the training process. Furthermore, as the training process progresses, contrastive learning through the explicitly decoupled semantic-related features yields higher mutual information compared to conducting contrastive learning alone. This indicates that our proposed semantic information decoupling module is capable of extracting the higher correlation features between visual and neural activities. Interestingly, we visualize the data of subjects 2,4,6 and 8 during training. The estimated MI values of these subjects show that the higher the MI values for the semantic-related features, the higher the testing accuracy on the test set. Particularly, subject 8, which exhibited the highest MI values during training, also performed the best top-1 and top-5 test accuracy among all subjects. The detailed analysis of the correlation between MI value and generalization performance is in Sec. IV-D. Higher MI values typically signify better feature correlation, which manifests as consistency between visual images and neural signals. By effectively learning these semantic-related features, we can enhance the performance in object recognition tasks and acquire more generalizable representations.

In the visualization of the cyclic consistency reconstruction module in Fig. 4(b), we find that the MSE score for the reconstruction of image features, comprising the image domain and EEG semantic parts, rapidly decreases and remains low during training. We suppose that this is an inherent property of the

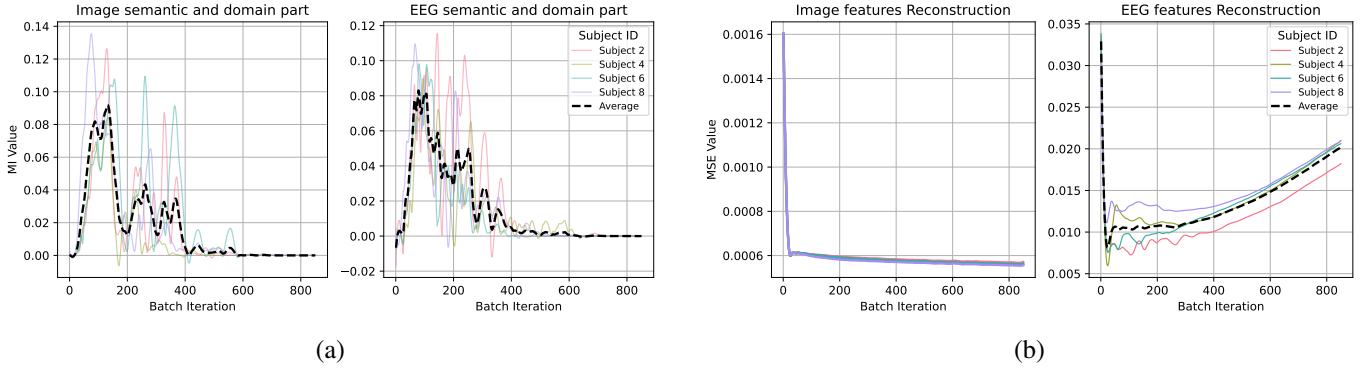


Fig. 4. Illustration of the MI values (smoothed) and MSE scores for VE-SDN during training batch iterations. (a) The mutual information estimated by CLUB between the semantic-related and domain-related parts of image and EEG features. (b) The MSE loss score of image and EEG part cyclic reconstruction.

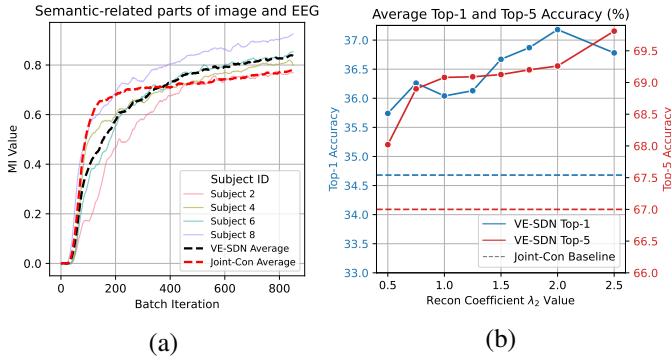


Fig. 5. (a) Illustration of the MI values (smoothed) between semantic-related parts of images and EEG. (b) Accuracy under different coefficient settings of λ_2 .

image domain features, as they contain a substantial amount of redundant pixel-level information, making the reconstruction of the original features relatively straightforward. However, in the EEG reconstruction part, the MSE score initially decreases rapidly but then gradually increases as training progresses. We think that this is due to EEG domain features typically containing a huge amount of noise. Although they are reconstructed using semantic-related features from images, there remains a substantial discrepancy from the original features, making effective reconstruction challenging. Nevertheless, as shown in Fig. 5(b), by increasing the weight coefficient of cyclic reconstruction during training, we can improve the average test accuracy for ten subjects in the downstream zero-shot classification task. This result indicates that increasing inter-modality semantic consistency during training can further enhance the performance of decoding.

D. Correlation between MI value and test accuracy

In this section, we explore how the MI values, derived from visual image and EEG features used in MCL, correlate with the accuracy of the test set. For ten subjects, we used approximate networks to estimate the sample average MI value of semantic-related features for each epoch and list the top-1 and top-5 accuracy for each epoch on the test set. We calculated the Pearson correlation coefficients (PCCs) between the MI values and both top-1 and top-5 accuracy across 50

TABLE II
INTRA-SUBJECT AVERAGE PEARSON CORRELATION COEFFICIENT (MEAN \pm STD.) BETWEEN THE SEMANTIC-RELATED MI VALUE AND 200-WAY ZERO-SHOT TEST ACCURACY

Intra-subject Pearson Correlation Coefficient		
Method	Average PCCs	
	Top-1	Top-5
Joint-Con	0.948 \pm 0.02	0.975 \pm 0.01
VE-SDN	0.973 \pm 0.006	0.974 \pm 0.009

TABLE III
INTER-SUBJECT PEARSON CORRELATION COEFFICIENT BETWEEN THE SUBJECT'S MI VALUE AND TEST ACCURACY

Inter-subject Pearson Correlation Coefficient		
Method	Top-1	Top-5
Joint-Con	0.780	0.789
VE-SDN	0.802	0.798

epochs for ten subjects and averaged these values. The results are shown in Table II; the PCCs values for both methods, Joint-Con and VE-SDN, indicate a significant positive correlation between the aligned feature MI values and the test accuracy, with significance at p -value < 0.001 . This indicates that within a subject, higher MI values correspond to greater consistency among features, thereby leading to higher decoding accuracy.

Furthermore, we explored the relationship between inter-subject MI values and generalization performance. We calculated the averages of MI values and test accuracy over the last 10 epochs for each subject as individual statistics data, and further computed the Pearson correlation coefficients between MI values and test accuracy across subjects. The results are shown in Table III; the PCCs value of top-1 accuracy of the two methods are 0.780 ($p < 0.05$) and 0.802 ($p < 0.05$), and top-5 PCCs are 0.789 ($p < 0.05$) and 0.798 ($p < 0.05$), also demonstrating a high positive correlation. These results indicate that subjects with higher MI values between visual and neural signals exhibit better decoding performance following MCL.

In summary, we find that whether intra-subject or inter-

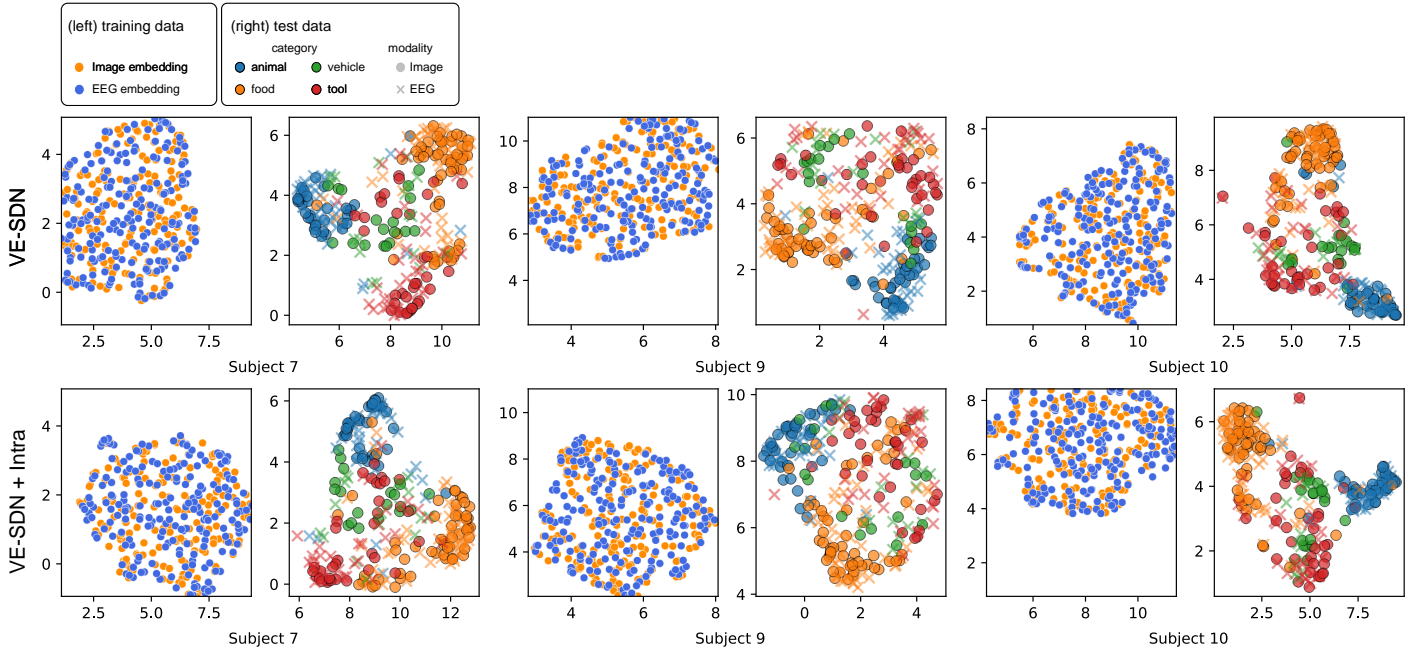


Fig. 6. Visualization of 200 randomly selected training sample pairs (left), along with the test visual images and EEG features (right) for subjects 7, 9, and 10, categorized into four groups. The display above shows the visualized features of VE-SDN after training, while the display below presents the visualized features with the incorporation of the intra-class geometric consistency.

subject, the MI values between visual images and EEG features are highly correlated with decoding performance. As analyzed in Sec. IV-C, enhancing the mutual information among features can improve the model’s decoding performance. This insight may offer new directions for the design of future decoding models.

E. Analysis on Intra-Class Geometric Consistency

Contrastive learning exhibits a powerful capability in multimodal representation learning, which effectively aligns the two modalities and can bring their distribution regions closer together. Modality alignment can be seen as a method to reduce the modality gap. Consequently, it is natural to aim to minimize the modality gap between positive pairs to achieve perfect alignment. However, [36] points out that exact modality matching does not yield performance gain according to both empirical and theoretical results. Therefore, instead of further reducing the modality gap, we propose an intra-class geometric consistency approach that reduces the variability in the modality gap between different visual samples and EEG prototypes within the same class. This is manifested as consistent Euclidean distances on the hypersphere. We suppose that intra-class geometric consistency offers two main benefits: 1. It prevents rapid changes in the modality distribution area on the hypersphere, thereby enhancing the stability of the model learning. 2. It prevents excessive reduction of sample distances, which avoids model overfitting to specific classes and improves its generalization ability. Empirical results indicate that employing intra-class geometric consistency during MCL enhances overall test classification accuracy. Additionally, we quantified the mutual information between semantic

features with added intra-class geometric consistency and found that the results are not notably different from those of pure contrastive learning. Therefore, maintaining consistency in this manner does not effectively increase the correlation between features. Conversely, it optimizes the geometric latent modality structure to improve the performance of downstream classification tasks.

As shown in Fig. 6, we display the 2D feature visualization for subjects 7, 9, and 10, who demonstrated improved accuracy by incorporating the intra-class geometric consistency into the VE-SDN method. Firstly, we randomly selected 200 training pairs of visual images and EEG samples, and visualized their embedding on a uniform scale. We found that models incorporating the intra-class geometric consistency approach (VE-SDN + Intra) showed cohesion and consistency in modality features. Then, we visualized the image and EEG embedding of four categories of samples in the test dataset. The features, especially for Subject 9, visualized by the VE-SDN + Intra method demonstrated improved intra-semantic class clustering and discrimination compared to those by VE-SDN alone.

F. Compare with state-of-the-arts approach

We conduct the main experiments on ThingsEEG datasets on the Zero-Shot neural decoding task. For a fair comparison, we do not introduce any label information by only comparing the VE-SDN model with the proposed models: 1) NICE [16], 2) ATM-E [18], and 3) ATM-S [18].

Our experiment and statistical methods refer to [18], utilizing the train and test image features provided therein. Given that previous methods differed in their data configurations (such as the source of the pre-trained model for image feature

TABLE IV
OVERALL TOP-1 AND TOP-5 ACCURACY (%) OF 200-WAY ZERO-SHOT CLASSIFICATION ON THINGS EEG DATASETS.

Method	Subject 1		Subject 2		Subject 3		Subject 4		Subject 5		Subject 6		Subject 7		Subject 8		Subject 9		Subject 10		Average	
	top-1	top-5	top-1	top-5	top-1	top-5	top-1	top-5	top-1	top-5	top-1	top-5	top-1	top-5	top-1	top-5	top-1	top-5	top-1	top-5	top-1	top-5
Subject dependent - train and test on one subject (batch size = 1024)																						
NICE	25.45	53.35	25.50	55.80	26.95	62.10	30.30	67.65	18.85	47.95	26.40	63.30	22.20	55.50	37.35	68.75	28.05	60.70	31.05	65.30	27.21	60.04
ATM-E	21.80	53.55	21.95	55.55	31.20	65.20	30.70	64.40	17.25	41.95	29.15	64.65	27.10	58.75	42.40	71.70	33.60	63.95	36.80	69.05	29.20	60.88
ATM-S	28.95	62.15	30.90	64.30	41.50	70.75	35.55	70.95	24.85	54.30	34.10	67.15	30.95	61.20	45.00	79.20	36.95	65.55	36.80	71.60	34.55	66.71
VE-SDN(ours)	32.55	63.65	34.40	69.90	38.65	73.45	39.75	72.00	29.35	58.60	34.45	68.80	34.50	68.30	49.30	79.75	39.00	69.60	39.80	75.30	37.18	69.94

extraction or whether the EEG training samples were averaged across repeated sessions), to facilitate a fair comparison and demonstrate the efficacy of our proposed method, we conducted each experiment using the same setting of training and testing samples, which averaging four repeated sessions of EEG training data to enhance sample quality. The total results are shown in Table IV.

In subject-dependent experiments, we found that averaging four repeated sessions of EEG training data within this configuration resulted in improved classification performance. The results demonstrate that our proposed method, VE-SDN, surpasses state-of-the-art methods in terms of top-1 and top-5 accuracy for nearly every subject. Overall, the average top-1 and top-5 accuracy across ten subjects increased by 2.63% and 3.23%, respectively.

Although the NICE and ATM methods also employ MLP projectors, they introduce residual connections to these projectors, thereby enabling identity mapping. This identity mapping does not eliminate the modality gap and feature discrepancy between visual images and EEG signals, which prevents further improvement in model performance. On the contrary, we only utilize a two-layer MLP to reproject visual images and EEG signals into a joint semantic space and align them through semantic consistency features to eliminate discrepancies between features, thereby further improving the performance of existing encoding models.

Compared to the ATM method, it is noteworthy that our approach enhances decoding performance by improving Visual-EEG Semantic Consistency without introducing additional textual information, which also demonstrates the effectiveness of our method.

G. Experiment on Supervised Contrastive Learning

We further utilize the inherent label information of Image-EEG pairs, employing Supervised Contrastive Learning (SupCon) [42] to replace Self-Supervised Contrastive Learning to align and maximize the mutual information between images and EEG features. As shown in Fig. 7, SupCon pulls samples that belong to the same class closer together in a mini-batch.

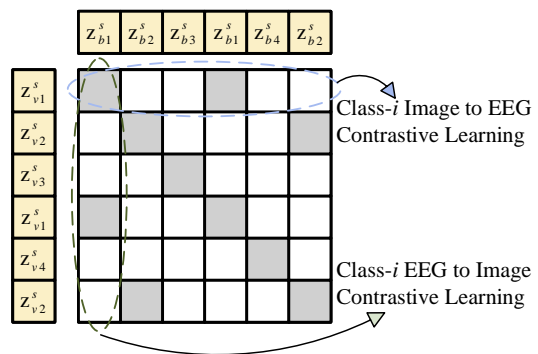


Fig. 7. Visualization the setting of Supervised Contrastive Learning.

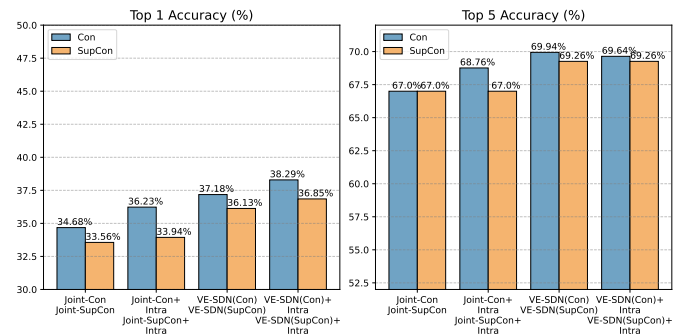


Fig. 8. Comparison of average top-1 and top-5 test accuracy of Contrastive Learning and Supervised Contrastive Learning.

Compared with Eq. (8), its modified form is as follows:

$$\begin{aligned}
 L_{supcon} = & \\
 & - \frac{1}{2} \sum_{i=1}^N \left[\frac{1}{\|P(i)\|} \sum_{p \in P(i)} \log \frac{\exp(f(z_{v,i}^s, z_{b,p}^s)/\tau)}{\sum_{j=1}^N \exp(f(z_{v,i}^s, z_{b,j}^s)/\tau)} \right. \\
 & \left. + \frac{1}{\|A(i)\|} \sum_{a \in A(i)} \log \frac{\exp(f(z_{b,i}^s, z_{v,a}^s)/\tau)}{\sum_{j=1}^N \exp(f(z_{b,i}^s, z_{v,j}^s)/\tau)} \right] \quad (17)
 \end{aligned}$$

where $P(i), A(i)$ represents all positive samples of another modality corresponding to anchor visual or EEG sample i in the current batch. The total results are shown in Figure 8, We found that incorporating inherent label information negatively



Fig. 9. Top-5 image retrieval results for five subcategories in the test set.

impacts the model’s generalization performance for Top-1 average test accuracy. Although it does not significantly affect Top-5 accuracy, it is still not as effective as pure contrastive learning. As discussed in Section IV-E, we speculate that the SupCon setting, by merely focusing on reducing intra-class distances, may cause the model to overfit to a specific class. This could impair the model’s performance in downstream prediction tasks, particularly with EEG signals. Also, the neural signals evoked by different stimulus images within the same category may also vary, which leads to suboptimal performance of the SupCon method in the neural decoding task.

Moreover, the decoupling framework VE-SDN and the intra-class geometric consistency approach remain effective in SupCon, enhancing classification accuracy in supervised settings. This further demonstrates the efficacy of our proposed methods.

H. Semantic Similarity and Image Retrieval

We subdivide the 200 test object concepts into six major categories: animal, food, vehicle, tool, clothing, and others. We utilize subject 8 for analysis, calculating the cosine similarity between pairwise EEG and image semantic features, and present the resulting representational similarity matrix as shown in Fig. 10. We observe that there is an intra-semantic class clustering between semantic-related EEG and image features, which indicates that the model is able to focus more on the semantic similarity between visual images and neural activity.

Additionally, we randomly selected two samples from each of the five subcategories for image retrieval analysis and listed the top five decoding results. As shown in Fig. 9, the top five images show semantic relevance, particularly in the categories of animals, food, and clothing.

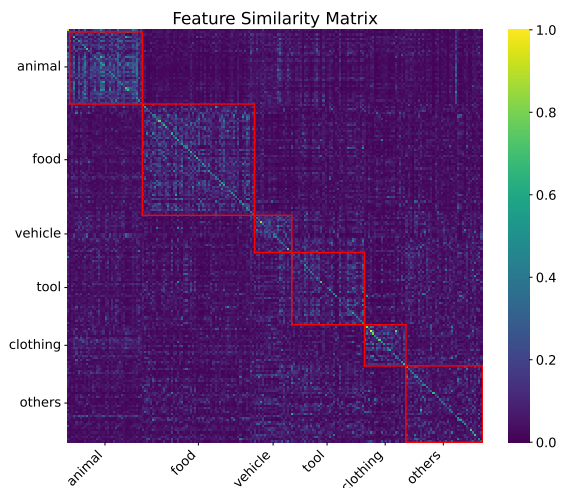


Fig. 10. Representation similarity matrices for EEG and image semantic features across six subcategories within 200 test concepts.

V. CONCLUSION

In this paper, beginning with the feature aspect of multimodal contrastive learning, we explore consistent semantic features between visual information and neural signals to enhance the performance of models decoding natural objects from human EEG signals. We propose a Visual-EEG Semantic Decouple Framework, which reprojects visual images and EEG signals into a joint semantic space, then explicitly decouples and aligns the semantic-related part of these two modality features. By quantifying the mutual information values between the semantic features of images and EEG, we found that both intra-subject and inter-subject with higher mutual information typically exhibit better decoding accuracy. Additionally, our proposed VE-SDN enhances the MI values

between visual image and EEG features, thereby further improving the decoding performance. Furthermore, we introduce an intra-class geometric consistency method to optimize the latent modality structure among features during MCL, as a result enhancing the robustness of the model. Experiments on large-scale Visual-EEG datasets demonstrate the effectiveness of our proposed methods.

REFERENCES

- [1] N. Kriegeskorte and P. K. Douglas, "Cognitive computational neuroscience," *Nature neuroscience*, vol. 21, no. 9, pp. 1148–1160, 2018.
- [2] X. Gao, Y. Wang, X. Chen, and S. Gao, "Interface, interaction, and intelligence in generalized brain–computer interfaces," *Trends in cognitive sciences*, vol. 25, no. 8, pp. 671–684, 2021.
- [3] F. R. Willett, D. T. Avansino, L. R. Hochberg, J. M. Henderson, and K. V. Shenoy, "High-performance brain-to-text communication via handwriting," *Nature*, vol. 593, no. 7858, pp. 249–254, 2021.
- [4] D. Liu, W. Dai, H. Zhang, X. Jin, J. Cao, and W. Kong, "Brain-machine coupled learning method for facial emotion recognition," *IEEE Transactions on Pattern Analysis and Machine Intelligence*, 2023.
- [5] A. Y. Wang, K. Kay, T. Naselaris, M. J. Tarr, and L. Wehbe, "Better models of human high-level visual cortex emerge from natural language supervision with a large and diverse dataset," *Nature Machine Intelligence*, vol. 5, no. 12, pp. 1415–1426, 2023.
- [6] C. Spampinato, S. Palazzo, I. Kavasidis, D. Giordano, N. Souly, and M. Shah, "Deep learning human mind for automated visual classification," in *Proceedings of the IEEE conference on computer vision and pattern recognition*, 2017, pp. 6809–6817.
- [7] W. Wang, F. Qi, D. P. Wipf, C. Cai, T. Yu, Y. Li, Y. Zhang, Z. Yu, and W. Wu, "Sparse bayesian learning for end-to-end eeg decoding," *IEEE Transactions on Pattern Analysis and Machine Intelligence*, vol. 45, no. 12, pp. 15 632–15 649, 2023.
- [8] H. Altaheri, G. Muhammad, and M. Alsulaiman, "Physics-informed attention temporal convolutional network for eeg-based motor imagery classification," *IEEE Transactions on Industrial Informatics*, vol. 19, no. 2, pp. 2249–2258, 2022.
- [9] Y. Song, Q. Zheng, B. Liu, and X. Gao, "Eeg conformer: Convolutional transformer for eeg decoding and visualization," *IEEE Transactions on Neural Systems and Rehabilitation Engineering*, vol. 31, pp. 710–719, 2022.
- [10] T. Horikawa and Y. Kamitani, "Generic decoding of seen and imagined objects using hierarchical visual features," *Nature communications*, vol. 8, no. 1, p. 15037, 2017.
- [11] J. Chen, Y. Qi, Y. Wang, and G. Pan, "Bridging the semantic latent space between brain and machine: Similarity is all you need," in *Proceedings of the AAAI Conference on Artificial Intelligence*, vol. 38, no. 10, 2024, pp. 11 302–11 310.
- [12] H. Ahmed, R. B. Wilbur, H. M. Bharadwaj, and J. M. Siskind, "Object classification from randomized eeg trials," in *Proceedings of the IEEE/CVF Conference on Computer Vision and Pattern Recognition*, 2021, pp. 3845–3854.
- [13] S. Palazzo, C. Spampinato, I. Kavasidis, D. Giordano, J. Schmidt, and M. Shah, "Decoding brain representations by multimodal learning of neural activity and visual features," *IEEE Transactions on Pattern Analysis and Machine Intelligence*, vol. 43, no. 11, pp. 3833–3849, 2020.
- [14] C. Du, K. Fu, J. Li, and H. He, "Decoding visual neural representations by multimodal learning of brain-visual-linguistic features," *IEEE Transactions on Pattern Analysis and Machine Intelligence*, 2023.
- [15] Y. Liu, Y. Ma, W. Zhou, G. Zhu, and N. Zheng, "Brainclip: Bridging brain and visual-linguistic representation via clip for generic natural visual stimulus decoding," 2023.
- [16] Y. Song, B. Liu, X. Li, N. Shi, Y. Wang, and X. Gao, "Decoding natural images from eeg for object recognition," *arXiv preprint arXiv:2308.13234*, 2023.
- [17] Y. Bai, X. Wang, Y.-p. Cao, Y. Ge, C. Yuan, and Y. Shan, "Dreamdiffusion: Generating high-quality images from brain eeg signals," *arXiv preprint arXiv:2306.16934*, 2023.
- [18] D. Li, C. Wei, S. Li, J. Zou, and Q. Liu, "Visual decoding and reconstruction via eeg embeddings with guided diffusion," *arXiv preprint arXiv:2403.07721*, 2024.
- [19] T. Fei and V. de Sa, "Image reconstruction from electroencephalography using latent diffusion," *arXiv preprint arXiv:2404.01250*, 2024.
- [20] V. W. Liang, Y. Zhang, Y. Kwon, S. Yeung, and J. Y. Zou, "Mind the gap: Understanding the modality gap in multi-modal contrastive representation learning," *Advances in Neural Information Processing Systems*, vol. 35, pp. 17 612–17 625, 2022.
- [21] T. M. Sutter, I. Daunhauer, and J. E. Vogt, "Generalized multimodal ELBO," in *International Conference on Learning Representations*, 2021. [Online]. Available: <https://openreview.net/forum?id=5Y21V0RDBV>
- [22] J. L. Bellmund, P. Gärdenfors, E. I. Moser, and C. F. Doeller, "Navigating cognition: Spatial codes for human thinking," *Science*, vol. 362, no. 6415, p. eaat6766, 2018.
- [23] L. McInnes, J. Healy, and J. Melville, "Umap: Uniform manifold approximation and projection for dimension reduction," *arXiv preprint arXiv:1802.03426*, 2018.
- [24] J. J. DiCarlo, D. Zoccolan, and N. C. Rust, "How does the brain solve visual object recognition?" *Neuron*, vol. 73, no. 3, pp. 415–434, 2012.
- [25] A. T. Gifford, K. Dwivedi, G. Roig, and R. M. Cichy, "A large and rich eeg dataset for modeling human visual object recognition," *NeuroImage*, vol. 264, p. 119754, 2022.
- [26] R. Kobler, J.-i. Hirayama, Q. Zhao, and M. Kawanabe, "Spd domain-specific batch normalization to crack interpretable unsupervised domain adaptation in eeg," *Advances in Neural Information Processing Systems*, vol. 35, pp. 6219–6235, 2022.
- [27] S. Bagchi and D. R. Bathula, "Eeg-convtransformer for single-trial eeg-based visual stimulus classification," *Pattern Recognition*, vol. 129, p. 108757, 2022.
- [28] R. Li, J. S. Johansen, H. Ahmed, T. V. Ilyevsky, R. B. Wilbur, H. M. Bharadwaj, and J. M. Siskind, "The perils and pitfalls of block design for eeg classification experiments," *IEEE Transactions on Pattern Analysis and Machine Intelligence*, vol. 43, no. 1, pp. 316–333, 2020.
- [29] B. Kaneshiro, M. Perreau Guimaraes, H.-S. Kim, A. M. Norcia, and P. Suppes, "A representational similarity analysis of the dynamics of object processing using single-trial eeg classification," *Plos one*, vol. 10, no. 8, p. e0135697, 2015.
- [30] M. N. Hebart, A. H. Dickter, A. Kidder, W. Y. Kwok, A. Corriveau, C. Van Wicklin, and C. I. Baker, "Things: A database of 1,854 object concepts and more than 26,000 naturalistic object images," *PloS one*, vol. 14, no. 10, p. e0223792, 2019.
- [31] K. Won, M. Kwon, M. Ahn, and S. C. Jun, "Eeg dataset for rsvp and p300 speller brain-computer interfaces," *Scientific Data*, vol. 9, no. 1, p. 388, 2022.
- [32] S. Lees, N. Dayan, H. Cecotti, P. McCullagh, L. Maguire, F. Lotte, and D. Coyle, "A review of rapid serial visual presentation-based brain-computer interfaces," *Journal of neural engineering*, vol. 15, no. 2, p. 021001, 2018.
- [33] H. Xu, G. Ghosh, P.-Y. Huang, D. Okhonko, A. Aghajanyan, F. Metze, L. Zettlemoyer, and C. Feichtenhofer, "Videoclip: Contrastive pre-training for zero-shot video-text understanding," *arXiv preprint arXiv:2109.14084*, 2021.
- [34] Y. Zhang, H. Jiang, Y. Miura, C. D. Manning, and C. P. Langlotz, "Contrastive learning of medical visual representations from paired images and text," in *Machine Learning for Healthcare Conference*. PMLR, 2022, pp. 2–25.
- [35] A. Radford, J. W. Kim, C. Hallacy, A. Ramesh, G. Goh, S. Agarwal, G. Sastry, A. Askell, P. Mishkin, J. Clark *et al.*, "Learning transferable visual models from natural language supervision," in *International conference on machine learning*. PMLR, 2021, pp. 8748–8763.
- [36] Q. Jiang, C. Chen, H. Zhao, L. Chen, Q. Ping, S. D. Tran, Y. Xu, B. Zeng, and T. Chilimbi, "Understanding and constructing latent modality structures in multi-modal representation learning," in *Proceedings of the IEEE/CVF Conference on Computer Vision and Pattern Recognition*, 2023, pp. 7661–7671.
- [37] S. Goel, H. Bansal, S. Bhatia, R. Rossi, V. Vinay, and A. Grover, "Cyclip: Cyclic contrastive language-image pretraining," *Advances in Neural Information Processing Systems*, vol. 35, pp. 6704–6719, 2022.
- [38] P. Cheng, W. Hao, S. Dai, J. Liu, Z. Gan, and L. Carin, "Club: A contrastive log-ratio upper bound of mutual information," in *International conference on machine learning*. PMLR, 2020, pp. 1779–1788.
- [39] A. v. d. Oord, Y. Li, and O. Vinyals, "Representation learning with contrastive predictive coding," *arXiv preprint arXiv:1807.03748*, 2018.
- [40] L. Van der Maaten and G. Hinton, "Visualizing data using t-sne," *Journal of machine learning research*, vol. 9, no. 11, 2008.
- [41] I. Loshchilov and F. Hutter, "Decoupled weight decay regularization," *arXiv preprint arXiv:1711.05101*, 2017.
- [42] P. Khosla, P. Teterwak, C. Wang, A. Sarna, Y. Tian, P. Isola, A. Maschinot, C. Liu, and D. Krishnan, "Supervised contrastive learning," *Advances in neural information processing systems*, vol. 33, pp. 18 661–18 673, 2020.